ACS OMEGA

http://pubs.acs.org/journal/acsodf

Article

Seed-Mediated Synthesis of Gold Nanorods at Low Concentrations of CTAB

Ming-Zhang Wei, Tian-Song Deng,* Qi Zhang, Zhiqun Cheng, and Shiqi Li

Cite This: *ACS Omega* 2021, 6, 9188−9195

Read Online

ACCESS | Metrics & More | Article Recommendations | Supporting Information

ABSTRACT: Although gold nanorods capped with hexadecyltrimethylammonium bromide (CTAB) have been prepared through the seed-mediated method for their use in diagnostics and therapeutics, the toxicity of AuNRs@CTAB limits their practical applications in the biomedical field. In this work, the synthesis and tuning of gold nanorods at very low concentrations of CTAB (as low as 0.008 M) was successfully achieved by using the seed-mediated method. Furthermore, we managed to optimize the growth conditions by changing the amount of seeds, $AgNO_3$, and/or HCl. At low CTAB concentrations, gold nanorods with tunable size and aspect ratio, high monodispersity, and high purity were obtained and studied by UV−vis spectroscopy, transmission electron microscopy, and Mie−Gans theoretical calculations. This work revealed a method of nanoparticle growth that may be extended to synthesize other nanomaterials such as Ag, Cu, Pd, and Pt at such low CTAB concentrations.

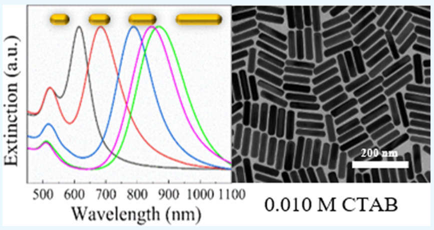

■ INTRODUCTION

Gold nanorods (AuNRs) have attracted many researchers in the recent two decades because of their special characteristics and wide applications, including chemical and biological sensing,[1−3] surface-enhanced Raman scattering (SERS),[4−6] anticancer therapy,[7−9] and imaging.[10−12] Optically, the interaction of free electrons with light at different wavelengths leads to the localized surface plasmon resonance (LSPR) effect.[13,14] It can be characterized by the scattering and absorption peaks corresponding to various wavelength ranges in the spectrum.[15] Furthermore, experimental results and theoretical calculations show that the LSPRs are directly related to the aspect ratio (length/diameter) of AuNRs (LSPR along the longitudinal direction contributes the most), and one can significantly control the aspect ratio of AuNRs by changing the amount of the reactant through the process of synthesis, which creates a wide spectral range from visible (∼600 nm) to the near-infrared region.[16−19]

Several synthesis methods of AuNRs have been developed, including chemical reduction,[20] electrochemical reduction,[21] and photochemical reduction.[22] A general and most used method is the seed-mediated method: Au^{3+} is fast reduced by sodium borohydride and turned into gold nanoparticles in the form of seeds in an aqueous hexadecyltrimethylammonium bromide (CTAB) solution. After the mild reduction of Au^{3+} in the growth solution by ascorbic acid, Au^0 directionally grows onto the seeds. This method was first proposed by El-Sayed and Nikoobakht in 2003[19] and further developed by Murray,[16] Murphy,[23] Wang,[18] and Liz-Marzán[24] groups. Through the process of AuNR synthesis, the concentration of CTAB has a great influence on the quality of the obtained products, including monodispersity, aspect ratio, and purity.[13] For this reason, suitable concentrations of CTAB should be considered to obtain a high quality and tunability of the AuNRs. Traditionally, a high concentration of CTAB (0.1 M) has been used in the seed-mediated growth processes.[19] In the work of Murray et al.,[16] the concentration of CTAB was lowered to 0.037 M by using binary surfactant mixtures, that is, the sodium oleate (NaOL) was introduced to function as another surfactant together with CTAB. This method greatly improved the dimensional tunability, monodispersity, and purity. Besides AuNRs, CTAB has been widely used in the synthesis of Cu,[25] Pd,[26] Pt,[27] and Ag[28] nanoparticles. By changing the types and concentration of reducing agents,[29] capping agents, and stabilizers,[30] different sizes and shapes of nanocrystals could be obtained. CTAB played the role of a capping and structure-directing agent and enhanced the anisotropic growth.[31,32] However, what cannot be ignored is the toxicity of CTAB combined with gold nanorods, which can cause serious damage to the biological cells and tissues. Ray et al.[33] carried out a series of experiments indicating that only a few cells (∼10%) could survive in the AuNRs@CTAB condition. Moreover, they mentioned that citrate-capped Au nanoparticles of different sizes are not inherently toxic to human skin cells, but AuNRs are highly toxic due to the presence of CTAB as a coating material. Guadagnini et al.[34] also demonstrated that some other nanoparticles like Fe_3O_4 coated with sodium oleate led to an unexpected increase in

Received: January 28, 2021
Accepted: March 16, 2021
Published: March 24, 2021

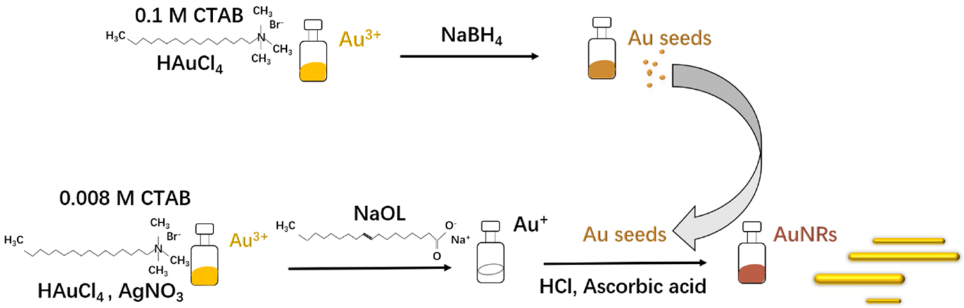

Figure 1. Schematic representation of the AuNR synthesis process at low CTAB concentrations.

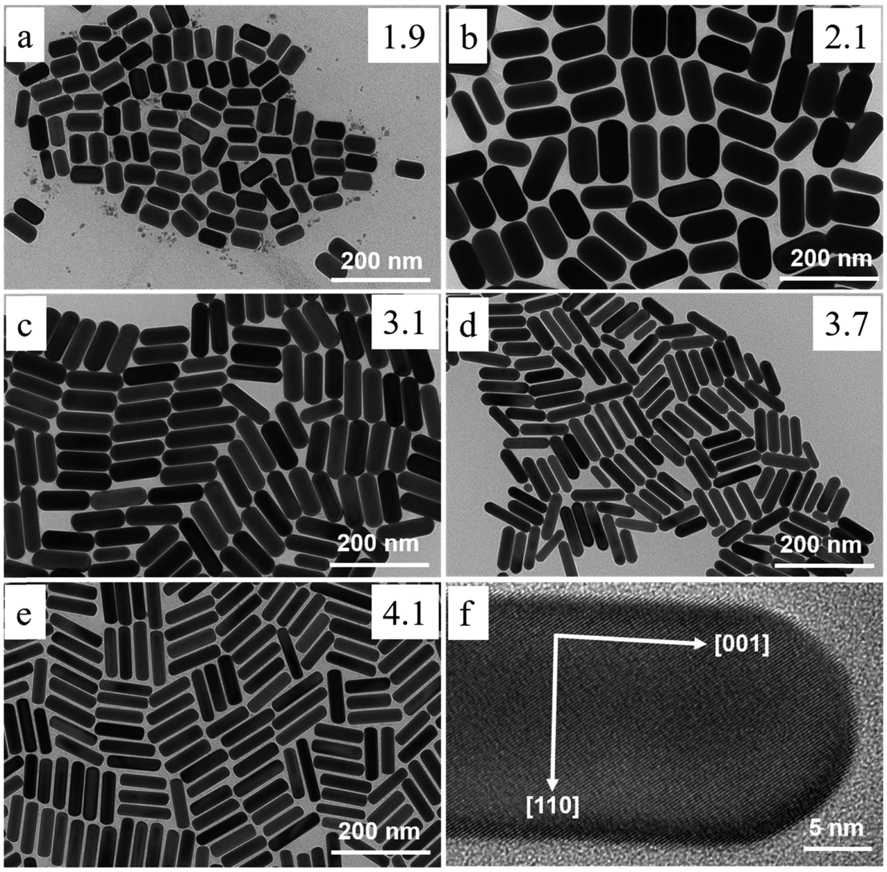

Figure 2. Morphology characterization of the AuNRs synthesized at low CTAB concentrations. (a−e) TEM images of the AuNRs synthesized at low concentrations of CTAB ((a) 0.008 M. (b−e) 0.01 M). The insets on the top right of (a)−(e) are the average aspect ratios of the AuNRs shown in the TEM images. Here, we mostly varied the AgNO$_3$ concentration and HCl addition to obtain different sizes of AuNRs, which are fully detailed in Table 1. (f) A high-resolution TEM (HRTEM) image of the AuNR. The sample is the same as in (e). The nanorod has the crystallographic ⟨001⟩ direction along the long axis of the rod and is observed to lie on the grid in a [110] projection, which is indicated by the white arrows in (f).

cytotoxicity. When the concentration of Fe$_3$O$_4$@NaOL was higher than 7 μg/cm^3, the metabolic activities of cells dropped precipitously. For reducing/removing the surfactants, e.g., CTAB and NaOL on the surface of AuNRs, some surface modification methods were carried out including AuNRs@mesoporous SiO$_2$[35] and AuNRs@poly(ethylene glycol) (PEG).[36] The advantage of using the mesoporous SiO$_2$ layer is that it enhances the stability of the AuNRs in solution.

Here, we report the seed-mediated growth of AuNRs at very low concentrations of CTAB (as low as 0.008 M, ∼20% of that in the previous work[16]) by using a binary surfactant (CTAB + NaOL). Simultaneously, the concentration of NaOL was also dropped to 5 mM (∼60% of that in the previous work[16]). Furthermore, we managed to optimize the growth conditions at low CTAB concentrations by changing the volumes of the seed solution, AgNO$_3$, and HCl. We characterized the obtained AuNRs by optical extinction spectra, transmission electron microscopy (TEM), and Mie−Gans calculations.

■ RESULTS AND DISCUSSION

AuNRs were synthesized by a modified seed-mediated method with binary surfactant mixtures.[16] Figure 1 shows a schematic process of the AuNR synthesis at 0.008 M CTAB. Firstly, the Au seeds were prepared by the reduction of HAuCl$_4$ using a strong reducing agent (NaBH$_4$). After aging for 30 min, the Au seeds were added to the growth solution containing the

Table 1. Average and Standard Deviations of the AuNR Size Parameters (Length, Diameter, and Aspect Ratio) Measured from the TEM Images and LSPR of the AuNR Samples Shown in Figure 2

CTAB (M)	NaOL (M)	HCl (mL)	$AgNO_3$ (mM)	seed (mL)	length (nm)	diameter (nm)	aspect ratio	LSPR (nm)	figure number
0.008	0.005	0.3	0.144	0.04	64.1 ± 7.7	34.9 ± 4.6	1.9 ± 0.2	615	Figure 2a
0.01	0.005	0.3	0.032	0.04	116.7 ± 11.6	56.1 ± 5.6	2.1 ± 0.3	684	Figure 2b
0.01	0.005	0.2	0.144	0.04	112.6 ± 9.4	36.8 ± 3.1	3.1 ± 0.4	789	Figure 2c
0.01	0.005	0.3	0.240	0.04	87.7 ± 10.1	23.7 ± 2.2	3.7 ± 0.5	846	Figure 2d
0.01	0.005	0.3	0.048	0.04	105.9 ± 9.0	26.2 ± 2.1	4.1 ± 0.5	869	Figure 2e

mixture of CTAB, NaOL, $HAuCl_4$, $AgNO_3$, and HCl. Finally, a mild reducing agent (ascorbic acid) was added and the solution was left undisturbed for nanorod growth (for more experimental details, see the Experimental Section and Supporting Information (SI)). The obtained AuNRs were characterized by optical extinction spectroscopy and TEM.

Figure 2a−e shows the TEM images of the AuNRs synthesized at low concentrations of CTAB (0.008 and 0.010 M). The amounts of NaOL, $AgNO_3$, HCl, and seeds are fully detailed in Table 1. By changing the growth condition, the aspect ratio of the obtained AuNRs could be tuned from 1.9 to 4.1. We determined the length, diameter, and aspect ratio of each sample by measuring around 200 (The maximum from Figure 2 is 300, determined by the AuNRs appearing in the TEM images.) nanorods from the corresponding TEM images. The average length, diameter, and aspect ratio are shown in Table 1. It can be observed from Figure 2 that although the CTAB concentration is very low, high-purity AuNRs with monodispersed shape were still obtained in this growth condition. Figure S1 shows a large-area TEM image of the same samples as in Figure 2e. Due to the high monodispersity, some of the nanorods self-assembled side-by-side on the copper grid. The inset in Figure S1 shows an optical image of the sample in a 40 mL vial (the total volume of the solution is ~25 mL).

To characterize the crystalline structure of the AuNRs, we performed high-resolution transmission electron microscopy (HRTEM) characterization for the sample in Figure 2e. Figure 2f shows a HRTEM image of the AuNR. The AuNR is a single crystal of face-centered cubic (fcc) structure, with one of the main axes oriented along the length of the rod. It is observed to lie on the copper grid in a [110] orientation, which is in agreement with previous reports.[37−39]

Figure 3 shows the extinction spectra of the AuNRs in Figure 2. The LSPR band wavelengths are at 615, 684, 789, 846, and 869 nm. There is still a wide range of tunability (from 615 to 869 nm) at the very low CTAB concentrations (0.008−0.010 M). The width of the LSPR peaks, which can be characterized by full width at half-maximum (fwhm), is quite sharp for each AuNR sample (e.g., fwhm = 52 nm, or 0.171 eV for the LSPR at 615 nm (black curve); fwhm = 99 nm, or 0.263 eV for the LSPR at 684 nm (red curve); fwhm = 126 nm, or 0.251 eV for the LSPR at 789 nm (blue curve); fwhm = 189 nm, or 0.328 eV for the LSPR at 846 nm (magenta curve); fwhm = 146 nm, or 0.240 eV for the LSPR at 869 nm (green curve)). The narrow fwhm further confirms that the obtained AuNRs have a high monodispersity.

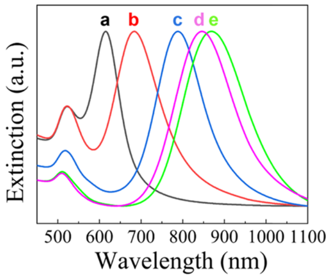

Figure 3. Normalized extinction spectra of the AuNRs shown in Figure 2a−e. The corresponding LSPR peaks are characterized in Table 1. The spectra are normalized to the extinction maximum.

To explore the size tunability of the AuNRs, we performed a series of experiments using different volumes of the seed solution at a fixed CTAB concentration (0.01 M). The other reactants were also kept unchanged and are fully detailed in Table 2. Figure 4a−e shows TEM images of the AuNRs synthesized with different amounts of seed particles. When the amount of seed particles was reduced, both the length and diameter of the AuNRs increased. When fewer seeds are available in the growth solution, the ratio of gold precursors/seeds increases. As every single seed binding site receives more number of gold precursors, it leads to the appearance of thicker and bigger AuNRs. A former research carried out by Murray et al.[16] also showed that less seed amounts in the final growth solution tended to produce thicker AuNRs using binary surfactants. Figure 4f shows the corresponding extinction spectra of the AuNRs shown in Figure 4a−e. Adding more seeds (from 0.005 to 0.16 mL) leads to an increase of the aspect ratio from 2.1 to 4.9 (Figure 4a−e). The increase of the aspect ratio is also reflected in a red shift of the LSPR peak from 709 to 896 nm (Figure 4f).

To investigate the plasmonic properties theoretically, we used the Mie−Gans theory[40] to calculate the extinction cross section of a single nanorod for the samples shown in Figures 2 and 4. We assumed that the AuNR has a spheroidal shape. Then, the extinction cross section can be obtained by an analytical expression (see eqs 1−6 in the Experimental Section). In the calculation, the size parameters were used as shown in Tables 1 and 2. More calculation details can be found in the Experimental Section. Figure S2 shows the extinction spectra of AuNRs by Mie−Gans calculation. The LSPR red-shifted as the aspect ratio increased. The characteristics of the calculated extinction spectra are in good agreement with the experimental spectra. However, the widths of the LSPR in the calculated spectra are sharper and the LSPR position is slightly different compared to the experimental data, which can be explained by the polydispersity of the experimental obtained nanorods, which was not taken into account in the single-particle calculations.

To fully control the synthesis of the AuNRs, we further investigated the influence of $AgNO_3$ and HCl on AuNR synthesis. First, we fixed the other parameters and only changed the concentration of $AgNO_3$ (from 0.016 to 0.48 mM) in the synthesis. All of the samples were synthesized with 0.01 M CTAB concentration. The experimental parameters are

Table 2. Average and Standard Deviations of the AuNR Size Parameters (Length, Diameter, and Aspect Ratio) Measured from the TEM Images and LSPR of the AuNR Samples Shown in Figure 4

CTAB (M)	NaOL (M)	HCl (mL)	$AgNO_3$ (mM)	seed (mL)	length (nm)	diameter (nm)	aspect ratio	LSPR (nm)	figure number
0.01	0.005	0.3	0.144	0.005	130.1 ± 13.0	60.8 ± 4.0	2.2 ± 0.3	709	Figure 4a
0.01	0.005	0.3	0.144	0.01	108.3 ± 11.4	42.3 ± 3.0	2.6 ± 0.4	736	Figure 4b
0.01	0.005	0.3	0.144	0.02	102.9 ± 9.7	35.2 ± 4.1	3.0 ± 0.5	765	Figure 4c
0.01	0.005	0.3	0.144	0.04	71.7 ± 9.2	20.9 ± 2.3	3.5 ± 0.7	793	Figure 4d
0.01	0.005	0.3	0.144	0.16	60.4 ± 11.3	12.9 ± 2.5	4.8 ± 1.0	896	Figure 4e

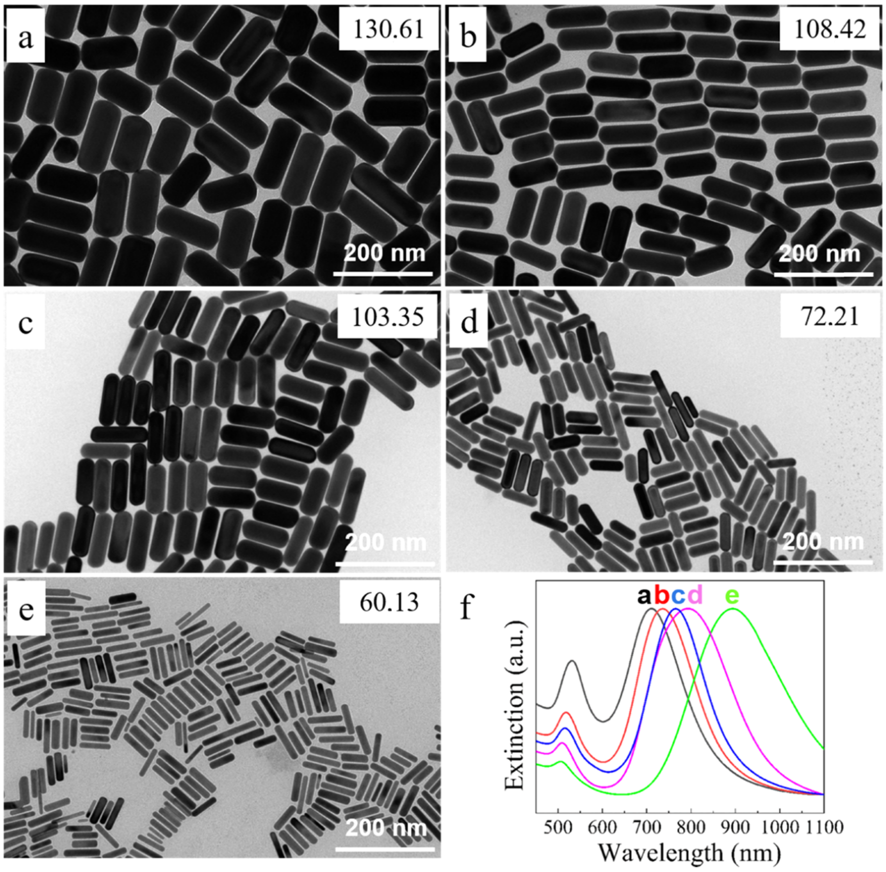

Figure 4. AuNRs synthesized by using different amounts of seed solution. (a−e) TEM images of AuNRs synthesized with different amounts of seeds. The insets on the top right of (a)−(e) show the length and diameter of the AuNRs. With the increase in amount of the seed particles, the size (both length and diameter) of the AuNRs reduced while the aspect ratio increased. (f) Normalized extinction spectra of the AuNRs shown in (a)−(e). The corresponding LSPR peaks are characterized in Table 1. The spectra are normalized to the extinction maximum.

listed in Table S1, and the extinction spectra are shown in Figure S3. There was an obvious increasing trend of the LSPR peaks from 653 to 889 nm at low concentrations of $AgNO_3$ (0.016−0.048 mM). However, at higher concentrations of $AgNO_3$ (>0.048 mM), the LSPR peak varied between 762 and 870 nm, showing an irregular change.

To evaluate the quality of AuNRs, Q and A_1/A_2 factors were defined. Here, $Q = \frac{\omega_0}{\Delta\omega} = \frac{\omega_0}{\omega_2 - \omega_1} = \frac{\lambda_1\lambda_2}{\lambda_0(\lambda_2 - \lambda_1)}$ where $\omega_0 = 2\pi c/\lambda_0$, $\omega_1 = 2\pi c/\lambda_1$, $\omega_2 = 2\pi c/\lambda_2$, c is the velocity of light in vacuum, λ_0 is the LSPR peak, and λ_1 and λ_2 are the wavelengths at half maximum of the LSPR peak. The parameter Q is widely used in electronics to describe the filter's filtering/passing capability for specific signal frequencies. The larger the parameter Q, the stronger the strobe ability of the circuit for a specific frequency of a signal and the greater the obstruction ability for other frequencies of the signal, which is reflected in the narrow bandwidth of the waveform. By transformation, the x-axis of the spectrum can be transformed into the frequency ($\omega = 2\pi c/\lambda$) and Q can be used to describe the bandwidth of the LSPR peaks instead of only the full width at half maximum. It is more precise and objective. Therefore, Q is a parameter that can reflect the monodispersity of AuNRs. In A_1/A_2, A_1 is the absorbance of the longitudinal LSPR peak and A_2 is the absorbance of the transverse LSPR/Au spheres peak. Khlebstov et al.[17] used A_1/A_2 to measure the purity of AuNRs. If a large quantity of Au spheres is obtained, the A_1/A_2 will be much lower than that for the normal AuNR samples. Although it is difficult to observe the trend of Q vs the $AgNO_3$ concentration, all the samples have high Q values (>4), as shown in Figure 5a. For the A_1/A_2 factor, it can be found that from 0.05 to 0.35 mM the A_1/A_2 values are high, indicating that the number of gold nanospheres in the synthesis process is relatively lower, which suggests a higher purity of the AuNRs. For the synthesis of AuNRs, the presence of Ag^+ is vital. It is believed to bond

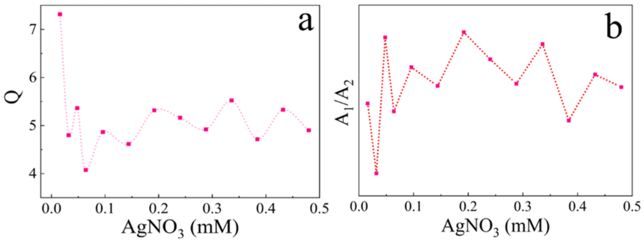

Figure 5. Quality analysis of the AuNRs synthesized at different concentrations of $AgNO_3$. (a) The parameter "Q" of gold NRs that were synthesized at $AgNO_3$ concentrations ranging from 0.016 to 0.48 mM. (b) A_1/A_2 in the same conditions as in (a). The amounts of other reactants are shown in Table S3. The LSPR peaks from 0.016 to 0.48 mM $AgNO_3$ concentration are listed in Table S1.

selectively to the {110} facets of Au nanocrystals and slow down the growth rate. Moreover, the tuning of AuNRs by adding different amounts of seed particles could not be achieved in the absence of Ag^+, leading to the appearance of Au particles with many different shapes.[41,42] The above series of experiments aimed at exploring a $AgNO_3$ concentration that is more suitable for the synthesis of AuNRs at a low concentration of CTAB (0.01 M). In our study, 0.05−0.35 mM $AgNO_3$ concentration was found to achieve a higher monodispersity and purity in the process of AuNR synthesis.

In addition to the $AgNO_3$, we also studied the effect of HCl in the synthesis. The experimental parameters are listed in Table S2, and the extinction spectra of the samples are shown in Figure S4. The LSPR peaks of 0.15, 0.2, 0.25, 0.3, 0.4, and 0.5 mL HCl addition amounts were 826, 782, 798, 864, 809, and 816 nm, respectively. Similar to the results of $AgNO_3$ mentioned above, there is no obvious trend of AuNR LSPR peaks with a single variation of HCl at a low concentration of CTAB (Figure S4a). When we further reduced the amount of HCl (0.1 and 0.15 mL of HCl in a 25 mL volume of the final solution), pure AuNRs could not be obtained (Figure S4b). Figure 6 shows the monodispersity and purity of AuNRs that were synthesized in different amounts of HCl through the parameters "Q" and A_1/A_2. It can be observed in Figure 6 that there is a good fit of the amounts of HCl (from 0.2 to 0.3 mL) for obtaining high-quality (both monodispersity and purity) AuNRs in this condition.

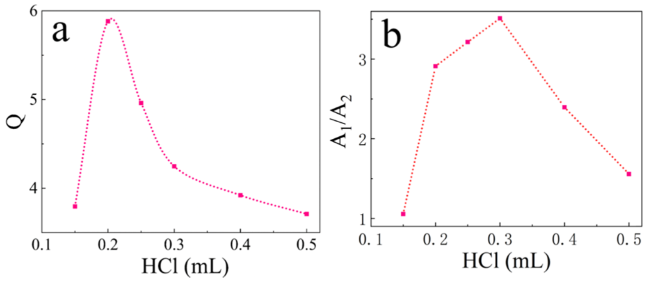

Figure 6. Quality analysis of the AuNRs synthesized with different amounts of HCl. (a) The parameter "Q" of gold NRs that were synthesized in 0.15−0.5 mL of HCl. (b) A_1/A_2 in the same conditions as in (a). The amounts of other reactants are listed in Table S3. The LSPR peaks from 0.15 to 0.5 mL HCl volume are listed in Table S2.

In the synthesis processes of AuNRs, HCl is introduced to adjust the pH. Series of studies have been done on the effect of pH in the process of AuNR synthesis, indicating that the good-fitting amount of HCl is essential for a good aspect ratio, monodispersity, and even shape of AuNRs. Researchers have proposed a hypothesis that the {110} facet of AuNRs would be packed densely by CTAB molecular bilayers and coated with AgBr, and the electrostatic attractive force between the bilayers and the AuNR surface is highly sensitive to the pH. With the increase of pH, a lesser number of CTAB−AgBr bilayers are found on the AuNR surface, and most AuNRs grow into different shapes.[43] However, whether this fits to the actual situation remains to be proved through further experimental work.

To test if this method can be scaled up, we carried out a 500 mL growth solution synthesis. The two samples shown in Figure S5 have exactly the same parameters as in Figure 2e. Both samples had a brownish color, which is the typical color for AuNRs. Furthermore, we carried out experiments at a much lower CTAB concentration and found that the 0.008 M concentration is very close to its limit. When we dropped the CTAB concentration to 0.006 and 0.005 M, the extinction spectra and optical images (Figure S6) confirmed that it failed to obtain high-quality AuNRs. A former work from Xu et al.[44] has proved that the key ingredient in directing the anisotropic growth of AuNRs is the complex CTA−Br−Ag^+. Thus, when the CTAB concentration is lowered to below 0.008 M, the concentration of the produced CTA−Br−Ag^+ is too low to ensure stable growth in this condition.

It should be noted that both similarities and differences exist when the results for the samples synthesized at a low CTAB concentration are compared with former works. One of the most notable differences is that the samples have become more pH sensitive (shown in Figure 6) and changes to the added amount of HCl affect the monodispersity and purity of the obtained AuNRs. After a series of experiments, we figured out that it is necessary to reduce the concentration of NaOL to 5 mM as well as vary the concentration of $AgNO_3$ to maintain a good monodispersity and tunability of the AuNRs (the NaOL concentrations in the previous works are 8 and 10 mM[16]). The differences mentioned above may due to the presence of CTAB, which preferentially binds to the middle of the AuNRs and renders a stabilizing power to the {100} facet that is proportional to the CTAB concentration.[13] When the CTAB concentration goes down, the stabilizing power is weakened and the growth condition becomes more sensitive to the synthesis parameters.

■ CONCLUSIONS

We have explored the seed-mediated synthesis and tuning of AuNRs at very low concentrations of CTAB by using CTAB + NaOL as the binary surfactant. The AuNRs can be obtained at as low as 0.008 M CTAB concentration, which is much lower than those in previous reports, e.g., 0.1 M from the El-Sayed group[19] and 0.037 M from the Murray group.[16] At 0.01 M CTAB concentration, we optimized the growth condition and successfully obtained AuNRs with size tunability, high monodispersity, and purity. Lesser seed amounts produced thicker nanorods. Moreover, AuNRs with higher quality were obtained at ∼0.05−0.35 mM $AgNO_3$ concentrations and 0.2−0.3 mL volume of HCl (in 25 mL growth solution). Compared to other methods, we directly reduced the CTAB concentration on the AuNR surface in the synthesis process while maintaining a high monodispersity and purity of the final products, which made it a direct template for practical applications. This method may improve the efficiency (e.g., simplify the wash cycles), lower the toxicity of the products, and can be extended to the synthesis of other nanomaterials such as Ag, Cu, Pd, and Pt at such low CTAB concentration.

■ EXPERIMENTAL SECTION

Materials. All chemicals were obtained from commercial suppliers and used without further purification. Hexadecyltrimethylammonium bromide (CTAB, >99.0%), chloroauric acid ($HAuCl_4$), and L-ascorbic acid (>99.99% metals basis) were purchased from Shanghai Macklin Biochemical Technology Co., Ltd. Silver nitrate ($AgNO_3$, >99.8%), sodium oleate (NaOL, >99.88%), and sodium borohydride ($NaBH_4$, >98%) were purchased from Shanghai Aladdin Biochemical Technology Co., Ltd.

Synthesis of Gold Nanorods. Seed solution: 0.25 mL of 10 mM $HAuCl_4$ was added to 10 mL of 0.1 M CTAB solution. Then, 0.6 mL of 10 mM $NaBH_4$ (freshly prepared with cold water) was added under vigorous stirring. The color of the solution changed from yellow to brownish yellow. The seed solution was aged at 30 °C for 30 min before use.

The growth solution was prepared by adding 2.5 mL of 0.1 M CTAB in a 40 mL scintillation vial. Then, 0.037 g of NaOL was dissolved in 21.25 mL of warm water (45−50 °C) in the same scintillation vial. When the solution cooled down to 30 °C, 0.9 mL of 4 mM $AgNO_3$ solution was added. The mixture was kept undisturbed at 30 °C for 15 min, after which 0.25 mL of 10 mM $HAuCl_4$ was added. The solution became colorless after 90 min of stirring. To adjust the pH, 0.3 mL of HCl (37 wt % in water) was added. 0.075 mL of 64 mM ascorbic acid and 0.04 mL of seed solution were added after 15 min. Finally, the resultant solution was left undisturbed at 30 °C for 12 h to grow. The final CTAB concentration was 0.01 M. The experimental parameters are listed in Tables 1 and 2, S1, and S2.

Characterization. Optical extinction spectra were recorded with a UV-1900i Spectrophotometer (Shimadzu, Japan) with a 10-mm optical path. Transmission electron microscopy (TEM) images were obtained with a HT-7700 microscope (Hitachi, Japan) operating at 100 kV. High-resolution TEM (HRTEM) images were obtained using a Tecnai 30F TEM (FEI) with a 300 kV acceleration voltage. The particle sizes of the AuNRs were measured from the TEM images, whereby >100 particles were measured for each sample.

To prepare the TEM samples, 1.5 mL of AuNR solution was centrifuged at 6000 rpm for 5 min. Then, the supernatant was removed and 1.5 mL of water was added (the concentration of CTAB was always kept higher than its CMC, ∼1 mM) and ultrasonicated for 10 min. The processes were repeated for three times. Finally, 5 μL of the solution in a centrifuge tube was drop-cast onto a carbon-coated 300 square-mesh copper grid and dried slowly in air.

Calculation of the Extinction Cross Section of the AuNRs. The extinction cross sections were calculated using the Mie−Gans theory.[40] Assuming AuNR has a spheroidal shape, the absorption (C_{abs}), scattering (C_{sca}), and extinction cross sections (C_{ext}) were obtained using the following analytical expressions

$$C_{\mathrm{abs}} = k\,\mathrm{Im}(\alpha) \tag{1}$$

$$C_{\mathrm{sca}} = \frac{k^4}{6\pi}|\alpha|^2 \tag{2}$$

$$C_{\mathrm{ext}} = C_{\mathrm{abs}} + C_{\mathrm{sca}} \tag{3}$$

where α is the polarizability corresponding to the long-axis excitation and $k = 2\pi\frac{\sqrt{\varepsilon_{\mathrm{m}}}}{\lambda}$ is the wave number. According to the Classius−Mossoti relation,[45] the polarizability α can be expressed as

$$\alpha = \frac{V\varepsilon_0(\varepsilon_{\mathrm{Au}} - \varepsilon_{\mathrm{m}})}{\varepsilon_{\mathrm{m}} + L(\varepsilon_{\mathrm{Au}} - \varepsilon_{\mathrm{m}})} \tag{4}$$

where V is the AuNR volume, ε_0 is the vacuum permittivity, $\varepsilon_{\mathrm{Au}}$ is the complex dielectric function of gold, and ε_{m} is the medium dielectric constant. L is the depolarization factor corresponding to the longitudinal direction and can be expressed as a function of the AuNR aspect ratio AR

$$L = \frac{1 - e^2}{e^2}\left(\frac{1}{2e}\ln\left(\frac{1 + e}{1 - e}\right) - 1\right) \tag{5}$$

$$e = \sqrt{1 - \frac{1}{\mathrm{AR}^2}} \tag{6}$$

In the calculations, the medium dielectric constant of water $\varepsilon_{\mathrm{m}} = 1.78$ was used and $\varepsilon_{\mathrm{Au}}$ was taken from Ciesielski et al.[46] The length and diameter of the AuNRs were obtained from the measurements of the TEM images (shown in Tables 1 and 2). The calculated extinction spectra are shown in Figure S2.

■ ASSOCIATED CONTENT

Supporting Information

The Supporting Information is available free of charge at https://pubs.acs.org/doi/10.1021/acsomega.1c00510.

> More TEM images and optical images of gold nanorods, extinction spectra by Mie−Gans calculations, experimental extinction spectra and tables by different synthesis conditions (PDF)

■ AUTHOR INFORMATION

Corresponding Author

Tian-Song Deng − *School of Electronics and Information Engineering, Hangzhou Dianzi University, Hangzhou 310018, China;* orcid.org/0000-0002-0841-4932; Email: dengts@pku.edu.cn

Authors

Ming-Zhang Wei − *School of Electronics and Information Engineering, Hangzhou Dianzi University, Hangzhou 310018, China*

Qi Zhang − *School of Electronics and Information Engineering, Hangzhou Dianzi University, Hangzhou 310018, China*

Zhiqun Cheng − *School of Electronics and Information Engineering, Hangzhou Dianzi University, Hangzhou 310018, China*

Shiqi Li − *School of Electronics and Information Engineering, Hangzhou Dianzi University, Hangzhou 310018, China*

Complete contact information is available at: https://pubs.acs.org/10.1021/acsomega.1c00510

Notes

The authors declare no competing financial interest.

■ ACKNOWLEDGMENTS

The authors acknowledge financial support from the National Science Foundation of China (NSFC, Grant no. 61905056) and Zhejiang Provincial Natural Science Foundation of China (Grant no. LY19E020011).

■ REFERENCES

(1) Xu, C. N.; Lan, L. Y.; Yao, Y.; Ping, J. F.; Li, Y. B.; Ying, Y. B. An unmodified gold nanorods-based DNA colorimetric biosensor with enzyme-free hybridization chain reaction amplification. *Sens. Actuator, B* **2018**, *273*, 642−648.

(2) Liu, G. L.; Feng, D. Q.; Qian, Y. L.; Wang, W.; Zhu, J. J. Construction of FRET biosensor for off-on detection of lead ions based on carbon dots and gold nanorods. *Talanta* **2019**, *201*, 90−95.

(3) Klinghammer, S.; Uhlig, T.; Patrovsky, F.; Bohm, M.; Schutt, J.; Putz, N.; Baraban, L.; Eng, L. M.; Cuniberti, G. Plasmonic Biosensor Based on Vertical Arrays of Gold Nanoantennas. *ACS Sens.* **2018**, *3*, 1392−1400.

(4) Wu, S. Y.; Shen, Y.; Jin, C. J. Surface-enhanced Raman scattering induced by the coupling of the guided mode with localized surface plasmon resonances. *Nanoscale* **2019**, *11*, 14164−14173.

(5) Matthews, J. R.; Shirazinejad, C. R.; Isakson, G. A.; Demers, S. M. E.; Hafner, J. H. Structural Analysis by Enhanced Raman Scattering. *Nano Lett.* **2017**, *17*, 2172−2177.

(6) Wu, L.; Garrido-Maestu, A.; Guerreiro, J. R. L.; Carvalho, S.; Abalde-Cela, S.; Prado, M.; Dieguez, L. Amplification-free SERS analysis of DNA mutation in cancer cells with single-base sensitivity. *Nanoscale* **2019**, *11*, 7781−7789.

(7) Yan, C. L.; Wang, Y. Y.; Tian, Q. W.; Wu, H. X.; Yang, S. P. Concentration effect on large scale synthesis of high quality small gold nanorods and their potential role in cancer theranostics. *Mater. Sci. Eng., C* **2018**, *87*, 120−127.

(8) Mao, W.; Son, Y. J.; Yoo, H. S. Gold nanospheres and nanorods for anti-cancer therapy: comparative studies of fabrication, surface-decoration, and anti-cancer treatments. *Nanoscale* **2020**, *12*, 14996−15020.

(9) Chen, J.; Li, X.; Zhao, X. L.; Wu, Q. Q.; Zhu, H. H.; Mao, Z. W.; Gao, C. Y. Doxorubicin-conjugated pH-responsive gold nanorods for combined photothermal therapy and chemotherapy of cancer. *Bioact. Mater.* **2018**, *3*, 347−354.

(10) Cai, K.; Zhang, W. Y.; Foda, M. F.; Li, X. Y.; Zhang, J.; Zhong, Y. T.; Liang, H. G.; Li, H. Q.; Han, H. Y.; Zhai, T. Y. Miniature Hollow Gold Nanorods with Enhanced Effect for In Vivo Photoacoustic Imaging in the NIR-II Window. *Small* **2020**, *16*, No. 2002748.

(11) Chen, Y. S.; Zhao, Y.; Yoon, S. J.; Gambhir, S. S.; Emelianov, S. Miniature gold nanorods for photoacoustic molecular imaging in the second near-infrared optical window. *Nat. Nanotechnol.* **2019**, *14*, 465−472.

(12) Cai, K.; Zhang, W. Y.; Zhang, J.; Li, H. Q.; Han, H. Y.; Zhai, T. Y. Design of Gold Hollow Nanorods with Controllable Aspect Ratio for Multimodal Imaging and Combined Chemo-Photothermal Therapy in the Second Near-Infrared Window. *ACS Appl. Mater. Interfaces* **2018**, *10*, 36703−36710.

(13) Chen, H. J.; Shao, L.; Li, Q.; Wang, J. F. Gold nanorods and their plasmonic properties. *Chem. Soc. Rev.* **2013**, *42*, 2679−2724.

(14) Perez-Juste, J.; Pastoriza-Santos, I.; Liz-Marzan, L. M.; Mulvaney, P. Gold nanorods: Synthesis, characterization and applications. *Coord. Chem. Rev.* **2005**, *249*, 1870−1901.

(15) Payne, E. K.; Shuford, K. L.; Park, S.; Schatz, G. C.; Mirkin, C. A. Multipole plasmon resonances in gold nanorods. *J. Phys. Chem. B* **2006**, *110*, 2150−2154.

(16) Ye, X. C.; Zheng, C.; Chen, J.; Gao, Y. Z.; Murray, C. B. Using Binary Surfactant Mixtures To Simultaneously Improve the Dimensional Tunability and Monodispersity in the Seeded Growth of Gold Nanorods. *Nano Lett.* **2013**, *13*, 765−771.

(17) Khlebstov, B. N.; Khanadeev, V. A.; Ye, J.; Sukhorukov, G. B.; Khlebtsov, N. G. Overgrowth of Gold Nanorods by Using a Binary Surfactant Mixture. *Langmuir* **2014**, *30*, 1696−1703.

(18) Ni, W. H.; Kou, X.; Yang, Z.; Wang, J. F. Tailoring longitudinal surface plasmon wavelengths, scattering and absorption cross sections of gold nanorods. *ACS Nano* **2008**, *2*, 677−686.

(19) Nikoobakht, B.; El-Sayed, M. A. Preparation and growth mechanism of gold nanorods (NRs) using seed-mediated growth method. *Chem. Mater.* **2003**, *15*, 1957−1962.

(20) Kimling, J.; Maier, M.; Okenve, B.; Kotaidis, V.; Ballot, H.; Plech, A. Turkevich method for gold nanoparticle synthesis revisited. *J. Phys. Chem. B* **2006**, *110*, 15700−15707.

(21) Zhou, Z.-Y.; Tian, N.; Huang, Z.-Z.; Chen, D.-J.; Sun, S.-G. Nanoparticle catalysts with high energy surfaces and enhanced activity synthesized by electrochemical method. *Faraday Discuss.* **2009**, *140*, 81−92.

(22) Ma, Y. Y.; Kuang, Q.; Jiang, Z. Y.; Xie, Z. X.; Huang, R. B.; Zheng, L. S. Synthesis of Trisoctahedral Gold Nanocrystals with Exposed High-Index Facets by a Facile Chemical Method. *Angew. Chem., Int. Ed.* **2008**, *47*, 8901−8904.

(23) Gole, A.; Murphy, C. J. Seed-mediated synthesis of gold nanorods: Role of the size and nature of the seed. *Chem. Mater.* **2004**, *16*, 3633−3640.

(24) González-Rubio, G.; Kumar, V.; Llombart, P.; Diaz-Nunez, P.; Bladt, E.; Altantzis, T.; Bals, S.; Pena-Rodriguez, O.; Noya, E. G.; MacDowell, L. G.; Guerrero-Martinez, A.; Liz-Marzán, L. M. Disconnecting Symmetry Breaking from Seeded Growth for the Reproducible Synthesis of High Quality Gold Nanorods. *ACS Nano* **2019**, *13*, 4424−4435.

(25) Wu, S. H.; Chen, D. H. Synthesis of high-concentration Cu nanoparticles in aqueous CTAB solutions. *J. Colloid Interface Sci.* **2004**, *273*, 165−169.

(26) Berhault, G.; Bausach, M.; Bisson, L.; Becerra, L.; Thomazeau, C.; Uzio, D. Seed-mediated synthesis of Pd nanocrystals: Factors influencing a kinetic- or thermodynamic-controlled growth regime. *J. Phys. Chem. C* **2007**, *111*, 5915−5925.

(27) Krishnaswamy, R.; Remita, H.; Imperor-Clerc, M.; Even, C.; Davidson, P.; Pansu, B. Synthesis of single-crystal line platinum nanorods within a soft crystalline surfactant-Pt-II complex. *ChemPhysChem* **2006**, *7*, 1510−1513.

(28) Khan, Z.; Al-Thabaiti, S. A.; Obaid, A. Y.; Al-Youbi, A. O. Preparation and characterization of silver nanoparticles by chemical reduction method. *Colloid Surf., B* **2011**, *82*, 513−517.

(29) Vigderman, L.; Zubarev, E. R. High-Yield Synthesis of Gold Nanorods with Longitudinal SPR Peak Greater than 1200 nm Using Hydroquinone as a Reducing Agent. *Chem. Mater.* **2013**, *25*, 1450−1457.

(30) Ye, X.; Gao, Y.; Chen, J.; Reifsnyder, D. C.; Zheng, C.; Murray, C. B. Seeded Growth of Monodisperse Gold Nanorods Using Bromide-Free Surfactant Mixtures. *Nano Lett.* **2013**, *13*, 2163−2171.

(31) Tao, A. R.; Habas, S.; Yang, P. Shape Control of Colloidal Metal Nanocrystals. *Small* **2008**, *4*, 310−325.

(32) Lim, B.; Jiang, M. J.; Tao, J.; Camargo, P. H. C.; Zhu, Y. M.; Xia, Y. N. Shape-Controlled Synthesis of Pd Nanocrystals in Aqueous Solutions. *Adv. Funct. Mater.* **2009**, *19*, 189−200.

(33) Wang, S.; Lu, W.; Tovmachenko, O.; Rai, U. S.; Yu, H.; Ray, P. C. Challenge in understanding size and shape dependent toxicity of gold nanomaterials in human skin keratinocytes. *Chem. Phys. Lett.* **2008**, *463*, 145−149.

(34) Guadagnini, R.; Moreau, K.; Hussain, S.; Marano, F.; Boland, S. Toxicity evaluation of engineered nanoparticles for medical applications using pulmonary epithelial cells. *Nanotoxicology* **2015**, *9*, 25−32.

(35) Gorelikov, I.; Matsuura, N. Single-step coating of mesoporous silica on cetyltrimethyl ammonium bromide-capped nanoparticles. *Nano Lett.* **2008**, *8*, 369−373.

(36) Niidome, T.; Yamagata, M.; Okamoto, Y.; Akiyama, Y.; Takahashi, H.; Kawano, T.; Katayama, Y.; Niidome, Y. PEG-modified

gold nanorods with a stealth character for in vivo applications. *J. Controlled Release* **2006**, *114*, 343−347.

(37) Wang, Z. L.; Mohamed, M. B.; Link, S.; El-Sayed, M. A. Crystallographic facets and shapes of gold nanorods of different aspect ratios. *Surf. Sci.* **1999**, *440*, L809−L814.

(38) Goris, B.; Bals, S.; Wouter, V. D. B.; Carbó-Argibay, E.; Gómez-Gra?a, S.; Liz-Marzán, L. M.; Van Tendeloo, G. Atomic-scale determination of surface facets in gold nanorods. *Nat. Mater.* **2012**, *11*, 930−935.

(39) Deng, T.; Hoeven, J. E. S. V. D.; Yalcin, A. O.; Zandbergen, H. W.; Huis, M. A. V.; Blaaderen, A. V. Oxidative Etching and Metal Overgrowth of Gold Nanorods within Mesoporous Silica Shells. *Chem. Mater.* **2015**, *27*, 7196−7203.

(40) Jain, P. K.; Eustis, S.; El-Sayed, M. A. Plasmon coupling in nanorod assemblies: optical absorption, discrete dipole approximation simulation, and exciton-coupling model. *J. Phys. Chem. B* **2006**, *110*, 18243−18253.

(41) Jana, N. R.; Gearheart, L.; Murphy, C. J. Seed-Mediated Growth Approach for Shape-Controlled Synthesis of Spheroidal and Rod-like Gold Nanoparticles Using a Surfactant Template. *Adv. Mater.* **2001**, *13*, 1389−1393.

(42) Busbee, B. D.; Obare, S. O.; Murphy, C. J. An Improved Synthesis of High-Aspect-Ratio Gold Nanorods. *Adv. Mater.* **2003**, *15*, 414−416.

(43) Cheng, J.; Ge, L.; Xiong, B.; He, Y. Investigation of pH Effect on Gold Nanorod Synthesis. *J. Chin. Chem. Soc.* **2011**, *58*, 822−827.

(44) Xu, Y.; Chen, L.; Ye, X. C.; Wang, X. C.; Yu, J. Q.; Zhao, Y.; Cao, M. H.; Xia, Z. H.; Sun, B. Q.; Zhang, Q. Cooperative interactions among CTA(+), Br- and Ag+ during seeded growth of gold nanorods. *Nano Res.* **2017**, *10*, 2146−2155.

(45) Kreibig, U.; Vollmer, M. *Optical Properties of Metal Clusters*; Springer-Verlag, 1995.

(46) Ciesielski, A.; Skowronski, L.; Trzcinski, M.; Gorecka, E.; Trautman, P.; Szoplik, T. Evidence of germanium segregation in gold thin films. *Surf. Sci.* **2018**, *674*, 73−78.

Supporting information for:

Seed-Mediated Synthesis of Gold Nanorods at Low Concentration of CTAB

Ming-Zhang Wei[1], **Tian–Song Deng**[1,*], **Qi Zhang**[1], **Zhiqun Cheng**[1], **Shiqi Li**[1]

[1]School of Electronics and Information Engineering, Hangzhou Dianzi University, No. 1158, 2nd Avenue, Baiyang Street, Hangzhou 310018, China

[*]Email: dengts@pku.edu.cn

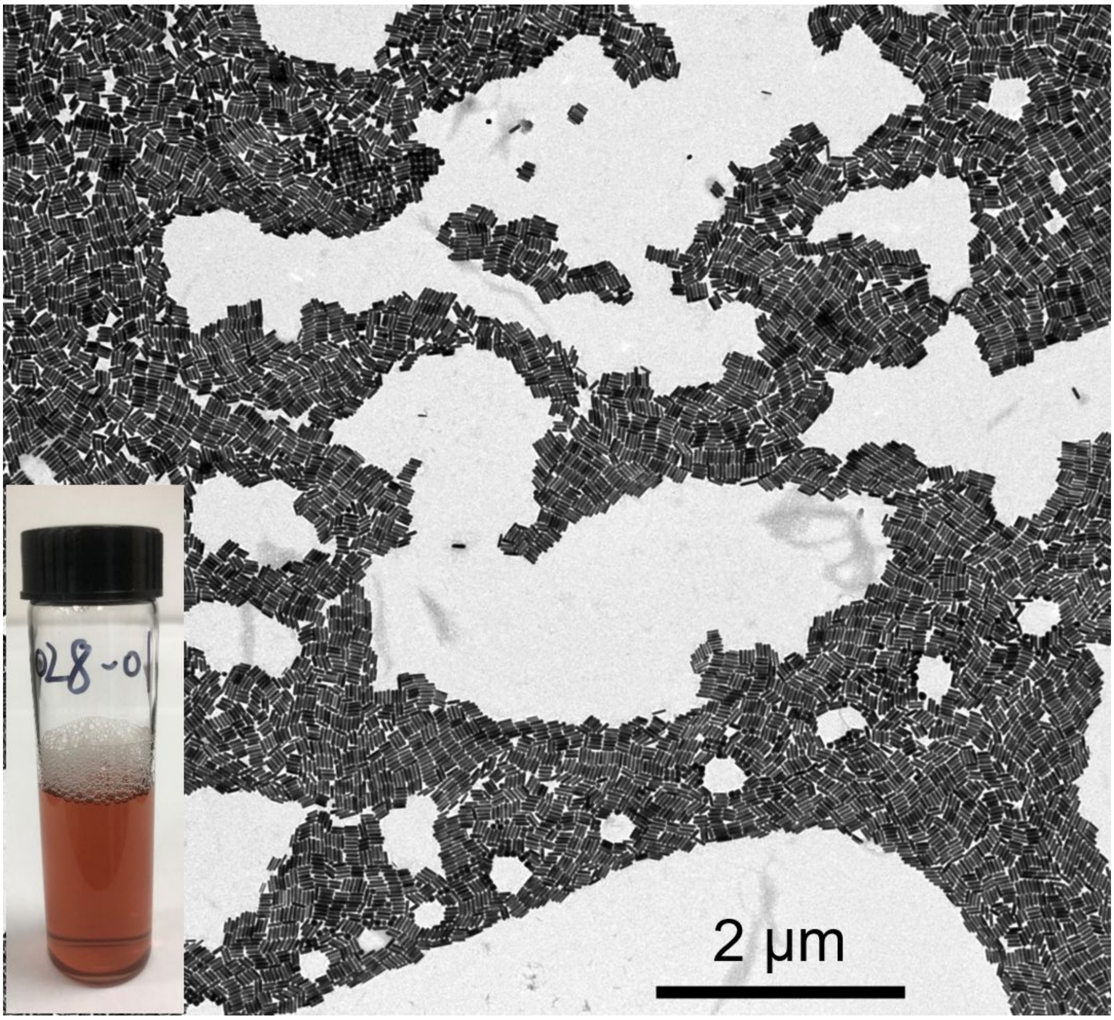

Figure S1. A large area TEM image of the same AuNRs shown in Figure 2e. The inset on the bottom-left is an optical image of the sample in a 40 mL vial. The length of the AuNRs is 105.9±9.0 nm, the diameter is 26.2±2.1 nm, and the aspect ratio is 4.1±0.5. The synthesis parameters are detailed in Table 1.

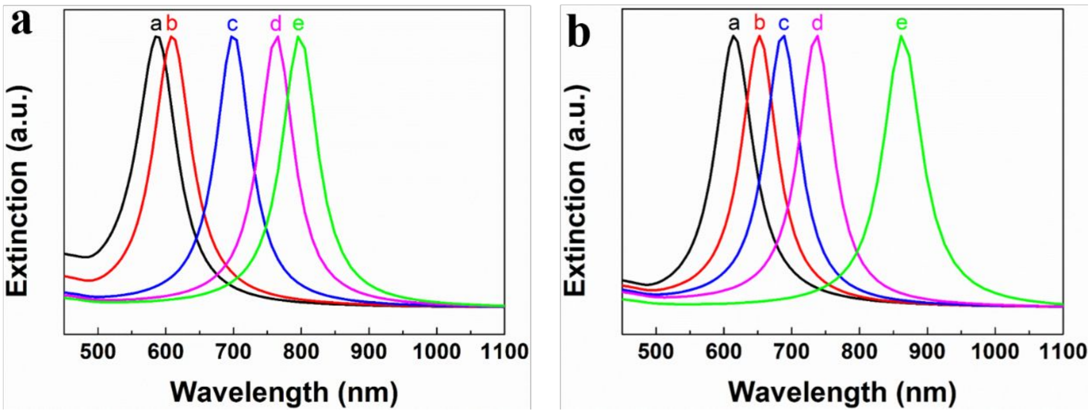

Figure S2. Normalized extinction spectra of AuNRs by Mie-Gans calculation: (a) corresponding samples from Figure 2a-e and (b) Figure 4a-e. Qualitatively, the experimental and calculated data have the same trend vs. aspect ratio and size effect. The misfit between them may arise from size polydispersity of the samples.

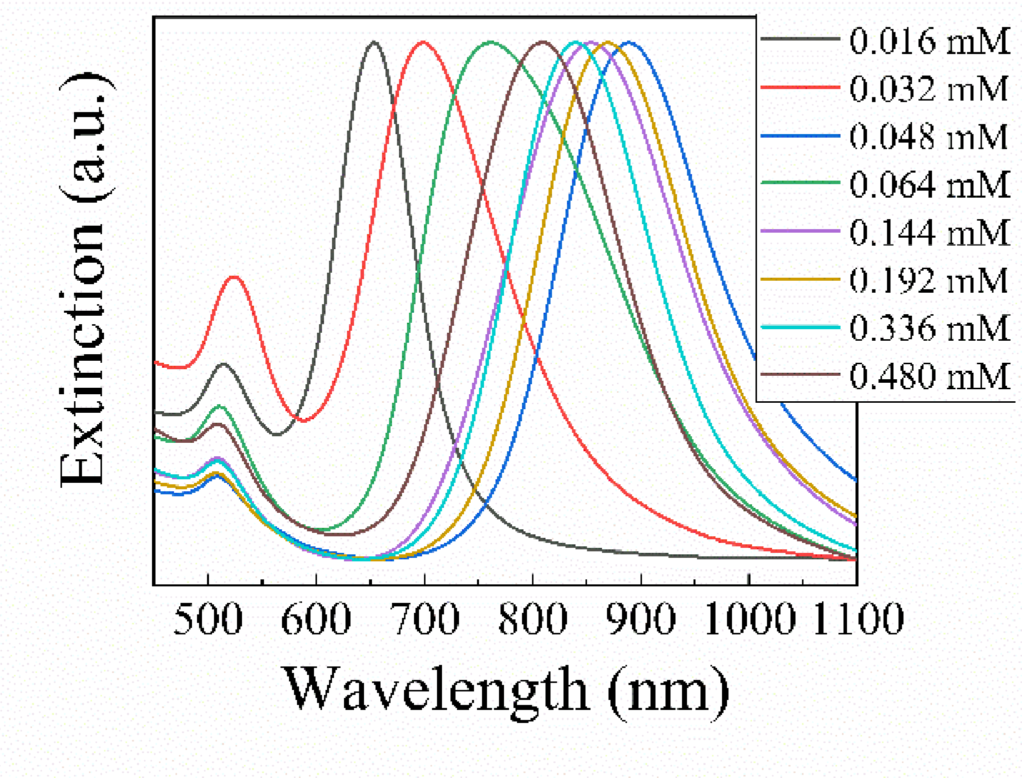

Figure S3. Normalized extinction spectra of AuNRs synthesized in the $AgNO_3$ concentrations from 0.016 mM to 0.48 mM. We removed some of the samples that the LSPR peaks overlapped.

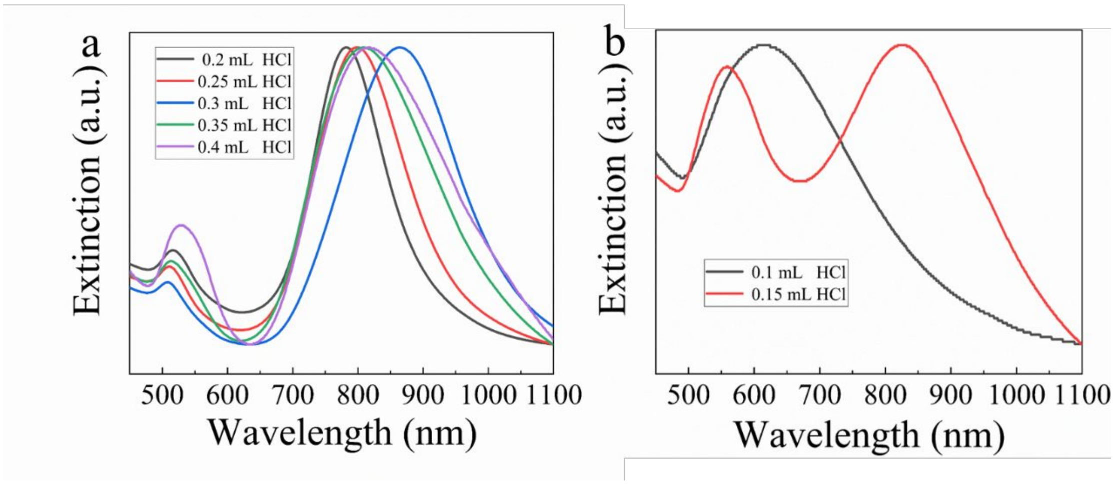

Figure S4. Normalized extinction spectra of AuNRs synthesized at different amounts of HCl. (a) Normalized extinction spectra of AuNRs synthesized in the HCl volume from 0.2 mL to 0.5 mL. (b) Normalized extinction spectra of AuNRs synthesized with the HCl volume of 0.1 mL (black) and 0.15 mL (red). The details of other reactants are listed in Table S2. The volume of final growth solution is 25 mL.

Figure S5. The optical images of AuNRs (500 mL of the final growth solution) under the same synthesis parameters as Figure 2e.

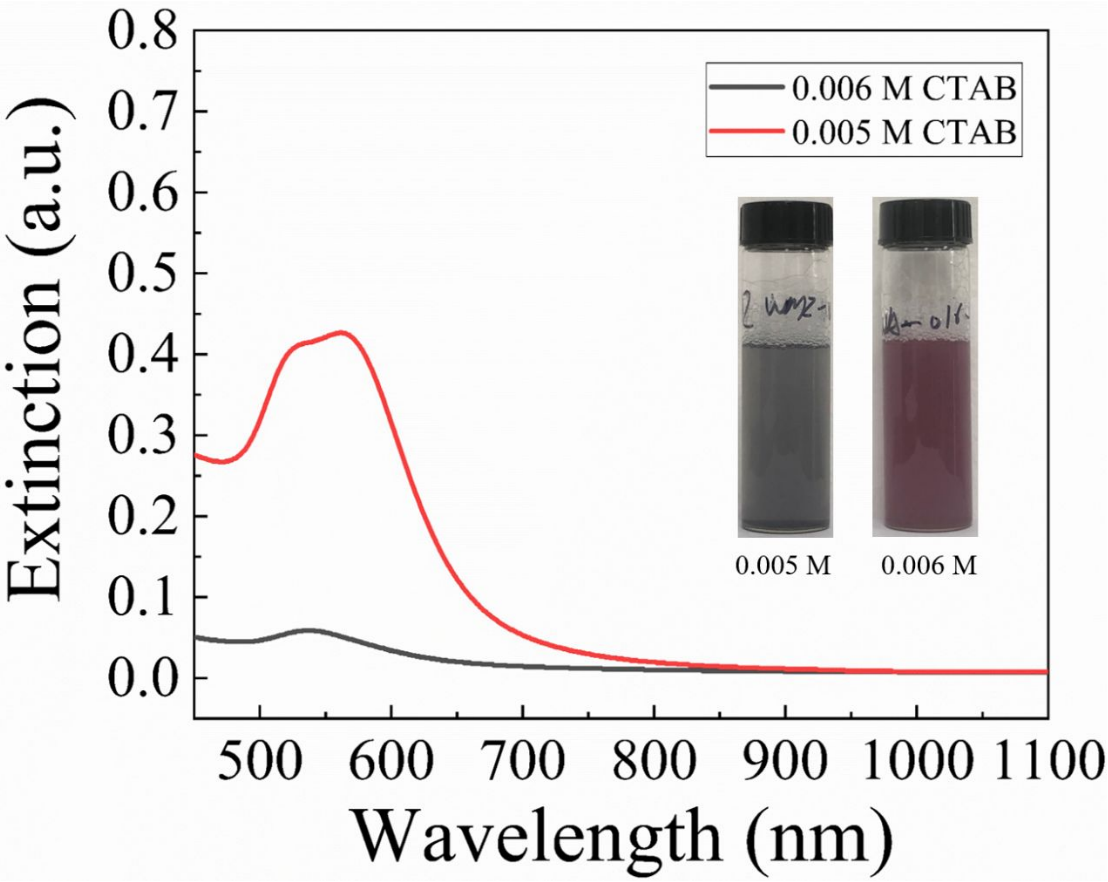

Figure S6. Extinction spectra and optical images of AuNRs synthesized at 0.005 M CTAB (red curve, 3 mM of NaOL, 0.144 mM of $AgNO_3$ and 0.6 mL of HCl), and 0.006 M CTAB concentration (black curve, 5 mM of NaOL, 0.144 mM of $AgNO_3$ and 0.3 mL of HCl).

Table S1. AuNRs synthesized at different volume of $AgNO_3$ in the final growth solution (The volume of the final growth solution is 25ml).

CTAB (M)	NaOL (M)	HCl (mL)	$AgNO_3$ (mM)	Seed (mL)	LSPR Peak (nm)	Figure Number
0.01	0.005	0.3	0.016	0.04	653	Figure 5
0.01	0.005	0.3	0.032	0.04	700	Figure 5
0.01	0.005	0.3	0.048	0.04	889	Figure 5
0.01	0.005	0.3	0.064	0.04	762	Figure 5
0.01	0.005	0.3	0.096	0.04	855	Figure 5
0.01	0.005	0.3	0.144	0.04	855	Figure 5
0.01	0.005	0.3	0.192	0.04	870	Figure 5
0.01	0.005	0.3	0.240	0.04	857	Figure 5
0.01	0.005	0.3	0.288	0.04	851	Figure 5
0.01	0.005	0.3	0.336	0.04	841	Figure 5
0.01	0.005	0.3	0.384	0.04	773	Figure 5
0.01	0.005	0.3	0.432	0.04	805	Figure 5
0.01	0.005	0.3	0.480	0.04	808	Figure 5

Table S2. AuNRs synthesized at different volume of HCl in the final growth solution (The volume of the final growth solution is 25ml).

CTAB (M)	NaOL (M)	HCl (mL)	$AgNO_3$ (mM)	Seed (mL)	LSPR Peak (nm)	Figure Number
0.01	0.005	0.1	0.144	0.04	618	Figure 6
0.01	0.005	0.15	0.144	0.04	826	Figure 6
0.01	0.005	0.2	0.144	0.04	782	Figure 6
0.01	0.005	0.25	0.144	0.04	798	Figure 6
0.01	0.005	0.3	0.144	0.04	864	Figure 6
0.01	0.005	0.4	0.144	0.04	809	Figure 6
0.01	0.005	0.5	0.144	0.04	816	Figure 6